Dehydration assessment via a portable, single sided magnetic resonance sensor

DR. ASHVIN BASHYAM (Orcid ID : 0000-0003-0541-5080)

Article type : Full Paper

Dehydration assessment via portable, single sided magnetic resonance sensor

Keywords: Portable magnetic resonance, dehydration, single-sided NMR, tissue fluid distribution, multicomponent T2 relaxometry, Unilateral Linear Halbach

Ashvin Bashyam[a,b], Chris J. Frangieh[a,b], Matthew Li[a,c], Michael J. Cima[a,d,*]

[a] *David H. Koch Institute for Integrative Cancer Research, Massachusetts Institute of Technology, Cambridge, MA, United States*

[b] *Department of Electrical Engineering & Computer Science, Massachusetts Institute of Technology, Cambridge, MA, United States*

[c] *Harvard-MIT Program of Health Sciences and Technology, Massachusetts Institute of Technology, Cambridge, MA, United States*

[d] *Department of Materials Science and Engineering, Massachusetts Institute of Technology, Cambridge, MA, United States*

[*] *Corresponding author. E-mail: mjcima@mit.edu*

Word count: 4961

Abstract

Purpose: Undiagnosed dehydration compromises health outcomes across many populations. Existing dehydration diagnostics require invasive bodily fluid sampling or are easily confounded by fluid and electrolyte intake, environment, and physical activity limiting widespread adoption. We present a portable

magnetic resonance (MR) sensor designed to measure intramuscular fluid shifts to identify volume depletion.

Methods: Fluid loss is induced via a mouse model of thermal dehydration (37 C, 15-20% relative humidity). We demonstrate quantification of fluid loss induced by hyperosmotic dehydration with multicomponent T2 relaxometry using both a benchtop NMR system and MRI localized to skeletal muscle tissue. We then describe a miniaturized (~1000 cm^3) portable (~4 kg) magnetic resonance (MR) sensor (0.28 Tesla) designed to identify dehydration-induced fluid loss. T2 relaxometry measurements were performed using a CPMG pulse sequence in ~4 minutes.

Results: T2 values from the portable MR sensor exhibited strong (R^2 = 0.996) agreement with benchtop NMR spectrometer. Thermal dehydration induced weight loss of 4 to 11% over 5 to 10 hours. Fluid loss induced by thermal dehydration was accurately identified via whole-animal NMR and skeletal muscle. The portable MR sensor accurately identified dehydration via multicomponent T2 relaxometry.

Conclusion: Performing multicomponent T2 relaxometry localized to the skeletal muscle with a miniaturized MR sensor provides a, non-invasive, physiologically relevant measure of dehydration induced fluid loss in a mouse model. This approach offers sensor portability, reduced system complexity, fully automated operation, and low cost compared to MRI. This approach may serve as a versatile and portable point of care technique for dehydration monitoring.

Introduction

Hyperosmotic dehydration traditionally refers to a total body water deficit often induced by a combination of restricted fluid intake and exposure to adverse environments (1). Fluid volume depletion is associated with poorer health outcomes when concomitant with chronic diseases, increased mortality among elderly and intensive care patients, decreased physical and cognitive performance, and impaired postoperative recovery (2–10).

Undiagnosed dehydration leads to negative health effects across many patient populations. Accurate and timely diagnosis is challenging as clinical presentation and symptoms are nonspecific and often present as an accompanying comorbidity to the primary diagnosis (1,7,11). For example, geriatric patients are highly susceptible to dehydration due to diminished thirst perception and plasma vasopressin (7,12–14). A diagnosis of dehydration in the elderly upon hospital admission increased 30-day post-admission

mortality rate by 80% (11). Soldiers are especially vulnerable to dehydration due to extended exposure in extreme environments, scenarios of intense stress where thirst perception is diminished, and limited water storage/transportation capabilities (15).

Despite the substantial health consequences of unmanaged dehydration, no accurate, robust, and practical assessment method currently exists (1,16). Commonly used vital signs and symptoms (e.g. headache, oral mucosa assessment, capillary refill time, skin turgor, fatigue) fail to provide a specific or objective assessment of dehydration (16–20). These diagnostic criteria do not provide an accurate measure of dehydration and are easily confounded by other comorbidities such as vascular disease, neurological deficit, and environmental conditions. Signs and symptoms of dehydration are often only apparent after fluid loss has progressed to severe stages.

Existing techniques involving sampling urine and/or blood, while clinically valid and accurate, are confounded by many factors, are invasive, require complex or time-consuming methods, and/or cannot be deployed in many settings (e.g. point of care) (21–25). Measurements of more easily accessible bodily fluids (e.g. saliva, tears, and sweat) exhibit substantial variability between individuals and are strongly biased by factors such as physical activity, food consumption, and humidity (26). Bioimpedance-based estimates of total body water as well as extracellular and intracellular fluid volumes fail to provide an actionable measure of fluid loss as its variability between individuals is substantial even when closely following measurement protocols (27–29). The variability of bioimpedance-based techniques is likely due to its reliance on an empirically derived model in healthy adults, which may not generalize to more diverse patient populations. Existing efforts to measure dehydration have focused on measurement of easily accessible, indirect physiological responses to fluid depletion. The inherently large variability in the response of individuals towards dehydration and a multitude of confounding factors limits the widespread adoption of these techniques (1).

There is a clear need for new approaches towards simple, non-invasive, and reliable measurement of fluid depletion. Desirable methods would interrogate and identify the underlying physiological response to dehydration, namely perturbations in the fluid distribution between tissues, and would not be based on population models (25).

Dehydration, specifically hyperosmotic dehydration, is characterized by a shift in the distribution of water within tissue fluid compartments driven by homeostatic regulation (30–34). Dehydration induces relatively large volume depletion of the intramuscular fluid compartments (extracellular and intracellular)

suggesting that a measurement of these tissue-specific fluid volumes could inform a diagnosis of dehydration (31). The extracellular fluid (ECF) compartment is more highly responsive to hyperosmotic fluid loss than the apparently conserved intracellular (ICF) compartment (31). ECF fluid depletion is driven primarily by fluid shifts from the interstitial space into the vascular space to maintain electrolyte and osmotic balance.

^{1}H NMR is exquisitely sensitive to the local physical and chemical environment of water molecules within the body (35). A T2-based MR measurement can provide information related to the composition and volume of a fluid compartment. Our group previously demonstrated that multicomponent T2 relaxometry via whole-body NMR can identify fluid depletion as a decrease in the signal amplitude from the lean tissue component (36). This led us to explore the localization of a similar measurement towards the skeletal muscle tissue with the ultimate goal of miniaturizing the magnetic resonance (MR) sensor.

Multicomponent T2 relaxometry via MRI has demonstrated sensitivity towards distinct fluid compartments within skeletal muscle tissue (37–39). These fluid compartments correspond to intracellular and extracellular water (40–43). The amplitudes recovered by multiexponential fitting reflect the absolute amount of water within the corresponding tissue fluid compartment contained within the sensing volume (40). For example, an increase in intramuscular ECF fluid volume, relative to the highly regulated ICF fluid compartment, would result in an increase in the amplitude attributed to the ECF. Lower extremity skeletal muscle offers an easily accessible site due to its relatively large size and a thin subcutaneous tissue layer for a portable MR sensor performing a localized measurement. A prior clinical study in hemodialysis (HD) patients from our group suggested that MRI localized to the skeletal muscle could identify fluid depletion (44). HD patients are hypervolemic but two of the healthy control subjects became dehydrated based on their blood chemistry (serum osmolality and sodium) and weight change. MRI measurements localized towards skeletal muscle within the leg showed sensitivity towards dehydration via a decrease in the intramuscular ECF amplitude. We hypothesized that a portable MR sensor designed to measure fluid shifts within this fluid compartment could reliably identify clinically meaningful volume depletion.

A portable, miniaturized MR-based platform for the diagnosis of dehydration is demonstrated in this study. We first characterize the ability of this single-sided MR sensor to perform high-sensitivity, remote multicomponent T2 relaxometry. We then show that multicomponent T2 relaxometry localized to the skeletal muscle, performed with a standard MRI system, is capable of quantifying fluid loss induced by dehydration in a mouse model. We further demonstrate that the portable MR system is capable of

localizing this measurement towards skeletal muscle tissue in vivo. Finally, we assess the ability of multicomponent T2 relaxometry performed with this portable sensor to measure dehydration supporting the preliminary findings from our previous clinical study. This technology provides an original approach towards measuring fluid volume status through a direct measure of the underlying physiology.

Methods

Study design

The objective of this study was to determine if multicomponent T2 relaxometry localized to the skeletal muscle could identify and quantify fluid loss in a mouse model of thermal dehydration to motivate the development of a portable sensor of fluid volume status. We developed a mouse model of thermal dehydration to induce fluid loss. We demonstrated that multicomponent T2 relaxometry via whole animal NMR can measure fluid loss. We performed multicomponent T2 relaxometry localized to muscle tissue via MRI to confirm our physiological hypothesis. We developed a portable MR sensor and characterized its ability to perform multicomponent T2 relaxometry over a spatially localized region. Finally, we show that our portable MR sensor can quantify dehydration through a localized measurement.

MR feature extraction and analysis methods were prospectively determined. Sample sizes were determined with power calculations based on effect sizes estimated from pilot experiments. No outliers were excluded from data analysis. Investigators were blinded to identity of mice while drawing regions of interest on MR images.

Mouse model of fluid loss induced by thermal dehydration

A mouse model of dehydration induced through exposure to elevated temperature (37 C) and airflow (15-20% relative humidity) combined with fluid restriction provided a model to examine fluid shifts in the skeletal muscle **(Fig. 1A)**. Dehydration induced by exposure to elevated temperatures preferentially depletes ECF over ICF (34).

Mice undergoing dehydration were weighed and scanned. Mice were then exposed to dehydrating conditions, weighed at regular intervals, and then scanned following 4-11% body weight loss. Control animals were at ambient conditions (20-22 C, 20-25% relative humidity, low airflow). An adjusted weight loss was computed by subtracting 3%, corresponding to losses from voiding, from the measured value which allowed the study to correlate the change in MR signal with weight loss induced only by thermal

dehydration. Animal studies were approved by the Massachusetts Institute of Technology Institutional Animal Care and Use Committee (0716-045-19). Additional information available in Supporting Information.

Multiexponential fitting for T2 relaxometry

CPMG T2 decay curves were estimated as multiexponential signals to extract relaxation times (τ_i) and relative amplitudes (A_i). A general multicomponent exponential decay signal is represented as:

$$\hat{y}(t,\boldsymbol{A},\boldsymbol{\tau}) = \sum_{\boldsymbol{i=1}}^{\boldsymbol{N}} \boldsymbol{A}_i * \exp\left(-t/\boldsymbol{\tau}_i\right) \quad \textbf{(1)}$$

where $\hat{y}(t)$ is the estimated signal, N is the number of components, $\boldsymbol{A}$ is a vector of amplitudes, and $\boldsymbol{\tau}$ is a vector of corresponding relaxation times. Two models were used to represent multicomponent signals. The first optimizes over both relaxation times and relative amplitudes. The optimal set of parameters is found by minimizing the L2-norm of the residuals between the estimated and the measured signal:

$$\boldsymbol{A}^{opt},\boldsymbol{\tau}^{opt} = \underset{\boldsymbol{A},\boldsymbol{\tau}}{\operatorname{argmin}} \|y(t) - \hat{y}(t)\|_2 \quad \textbf{(2)}$$

where $y(t)$ is the measured signal and $\|.\|_2$ represents the L2-norm. This model allows discovery of the relaxation times of a multiexponential signal. The second model optimizes only over relative amplitudes as the relaxation times are specified as parameters:

$$\boldsymbol{A}^{opt} = \underset{\boldsymbol{A}}{\operatorname{argmin}} \|y(t) - \hat{y}(t,\boldsymbol{\tau})\|_2 \quad \textbf{(3)}$$

This more constrained model allows amplitudes to be estimated more accurately. 95% confidence intervals for each parameter were computed assuming an asymptotic normal distribution for each estimate.

Whole animal NMR measurements

Whole animal multicomponent T2 relaxometry measurements performed via benchtop NMR relaxometry before and after dehydration **(Fig. 1B)** validated the animal model and demonstrated the utility of a MR measurement to identify dehydration. The ultimate goal was to develop a portable sensor to measure dehydration rather than requiring a whole body measurement. The ability to perform a localized measurement towards a specific tissue compartment was essential to allow for miniaturization of the MR sensor. We therefore explored the potential to localize a similar MR measurement to confine the relaxivity measurement to the muscle via MRI.

Intramuscular MRI measurements of fluid depletion

Quantitative T2 relaxometry measurements localized to skeletal muscle were performed before and after dehydration with a standard MRI scanner **(Fig. 1B)**. MRI scans were performed with a 7T/310/ASR (Agilent, formerly Varian) scanner with vnmrj software (version 3.2b), equipped with a 38 mm whole body coil. T2 weighted anatomical scans were performed with FSEMS (fast spin echo multi slice) and a series of spin echo images for T2 relaxometry were acquired with MEMS (multi echo multi slice). Additional information available in Supporting Information. Regions of interest (ROIs) were drawn manually on T2 weighted images to include skeletal muscle within the upper leg while excluding voxels primarily containing fat.

A biexponential fit with fixed relaxation times (**Eq. (3)** with τ_1 = 21 ms and τ_2 = 75 ms) was performed on the averaged decay curve to extract the relative amplitudes of fast (A_1) and slow (A_2) components. These relaxation times correspond to the mean relaxation times when performing a biexponential fit (**Eq. (2))** jointly across all images.

The utility of MRI as a diagnostic measure of dehydration is limited by its complexity, long measurement time, manual interpretation, high cost, and lack of portability. Therefore, we aimed to show that a comparable measurement performed by a portable MR sensor could identify fluid loss induced by dehydration while overcoming the limitations of MRI.

Portable MR sensor for remote, multicomponent T2 relaxometry

We designed a portable MR sensor with the goal of achieving high sensitivity measurements remote from the surface of the sensor to measure tissue fluid distribution. The portable MR sensor was designed and constructed with a permanent magnet array to generate a static magnetic field based on the Unilateral Linear Halbach array **(Fig. 2A-B)** (45,46). This sweet spot magnet design enables high sensitivity measurements over a large uniform region compared to more common high gradient designs (47–51). Permanent magnets provide a static magnetic field while also allowing for cost effectiveness, low maintenance, minimal power requirements, and portability compared to the more traditional superconducting magnets. Furthermore, the magnetic field is parallel to the sensor surface allowing for use of standard RF transceiver coils which maximizes sensitivity (46).

The static magnetic field profile of the portable MR sensor was measured by scanning a Hall probe (HMMT-6J04-VR, Lake Shore Cryotronics) connected to a gaussmeter (Model 475 DSP Gaussmeter) through a three-dimensional grid with 1 mm spacing. The magnet produces a uniform region with a field strength of 0.28 Tesla located 2 to 7 mm from the surface of the sensor as modeled by field simulations **(Fig. S1)** and experimentally confirmed with an acquired field profile **(Fig. 2C)**.

Two-dimensional sensitivity profiles of the system were characterized by measuring the relative signal amplitude from a sample scanned through the sensitive region **(Fig. 3A-B)**. A 2 mm spherical bulb of CuSO4 aqueous solution was scanned across the measurement plane. The amplitude of the peak corresponding to the solution indicated the signal strength originating from the contents of the bulb. The sensor is sensitive towards a region located directly above the RF coil spanning a 12 × 5 × 2 mm volume **(Fig. 3C-D)**. This allows localization of the measurement to skeletal muscle tissue while reducing confounding signal from subcutaneous tissue (52).

One compartment phantoms of varying $CuSO_4$ concentration were scanned with the portable MR sensor using a CPMG pulse sequence with 8192 echoes, an echo time of 65 μs, a repetition time of 1032.5 ms, an RF excitation frequency of 11.66 MHz, a pulse duration of 12 μs, an acquisition bandwidth of 2 MHz (dwell time of 0.5 μs), and 16 acquired points per echo with a Kea2 spectrometer (Magritek, Wellington, New Zealand). These results were compared to measurements via a benchtop NMR spectrometer (minispec mq20, Bruker, USA) using a CPMG pulse sequence with 65535 echoes, an echo time of 426 μs, a repetition time of 27.94 seconds, an RF excitation frequency of 19.95 MHz, an excitation pulse duration of 1.9 μs, an inversion pulse duration of 3.8 μs, an acquisition bandwidth of 1 MHz (dwell time of 3 μs), and 1 acquired point per echo.

A heterogeneous, synthetic tissue phantom with two compartments corresponding to unique T2 relaxation rates was constructed from 30 glass capillary tubes (1 mm diameter) arranged in a tightly packed circular formation. Two equal sets of tubes were filled with the requisite concentrations of aqueous $CuSO_4$ solution to produce T2 relaxation times of 24 ms (29 mM) and 84 ms (5 mM). The tubes were arranged randomly. Measurements were performed with parameters identical to those used in the previous experiment.. Amplitudes were extracted by fitting the decay curves with a biexponential model **(Eq. (2))**. Repeated trials were performed to yield histograms of estimation error. Additional information available in Supporting Information.

Portable MR measurements of fluid depletion

We performed T2 relaxometry with the portable MR sensor on the upper leg of mice to characterize its ability to identify systemic fluid depletion **(Fig. 4A)**. The signal originated primarily from the muscle tissue with some subcutaneous tissue and bone contribution **(Fig. 4B)**. The magnet geometry enables highly localized measurements over a remote region within mouse skeletal muscle. Anesthetized (2% isoflurane) mice were placed on the sensor in a prone position. The upper leg was positioned on the RF coil. A series of CPMG scans were acquired to perform T2 relaxometry (11.61 MHz B_1 frequency, 65 μs echo time, number of echoes 8192, 1 dummy echo, 1 MHz acquisition bandwidth, 12 μs pulse duration, 1.517 sec repetition time) until the signal to noise ratio of the resultant mean signal exceeded 150. A triexponential fit with fixed relaxation times (**Eq. (3)** with τ_0 = 1 ms, τ_1 = 50 ms, τ_2 = 150 ms) was performed to extract the relative amplitudes of fast (A_0), medium (A_1), and slow (A_2) components. These relaxation times correspond to the mean relaxation times when performing a triexponential fit (**Eq. (2)**) jointly across all scans.

Statistical analysis

Statistics for linear fits established significance through two-sided t test of linear model coefficients with a significance value of 5%. Independence and normality of the residuals was tested. Normality was established through a Lilliefors goodness-of-fit test of composite normality with a significance value of 5%. A Mann-Whitney U-test was used when samples were not normally distributed. Errorbars for parameters defining exponential fits indicate normal-based 95% confidence intervals on parameter estimates. For box and whisker plots, the centerline indicates the median, the limits of the box indicate 25th and 75th percentiles, and the limits of the whiskers indicate the minimum and maximum values.

Results

Mouse model of fluid loss induced by thermal dehydration

Fluid loss of between 4 and 11% body weight was induced over the 5 to 10 hour experimental period in experimental mice. Control animals experienced a mean weight loss of 3% body weight despite no exposure to elevated temperature and no restriction of food and water intake. This fluctuation in weight was likely due to voiding of urine and feces due to disruption of regular diurnal cycle and stress due to handling (53–55). These animals likely maintained euvolemia due to their unrestricted access to food and water.

Whole animal multicomponent T2 via benchtop NMR relaxometry demonstrated the utility of a MR measurement to identify dehydration **(Fig. S2, Fig. S3).** Additional information available in Supporting Information.

Intramuscular MRI measurements of fluid depletion

T2-weighted MR images of the leg were used to draw muscle tissue regions of interest (ROI) **(Fig. 5A)**. The upper leg was selected as it contains the largest skeletal muscles. A ROI was drawn to isolate voxels comprised principally of muscle tissue. The series of spin echo images provide a T2 decay curve capable of quantitatively identifying variation in relaxation rate **(Fig. S4)**. A composite T2 decay signal was formed from voxels corresponding to muscle tissue **(Fig. 5B)**. The noise distribution in each decay curve was transformed from Rician to Gaussian to reduce bias in estimation of the relaxation times **(Fig. S5A)** (56). These signals indicate a decrease in decay time (pre: 58 ms; post: 47 ms) after dehydration. The long component of the biexponential T2 signal corresponds to the intramuscular ECF compartment (40–43). The residuals of a biexponential fit are independent and identically distributed with a mean of zero. This suggests that the underlying signal can be completely described by a two-component model.

The estimated fluid volume attributed to the intramuscular ECF decreases significantly after dehydration ($n = 33$, $p < 1\times10^{-6}$, statistics by t test) while not changing among control animals ($n = 9$, $p < 0.5820$, statistics by t test) **(Fig. 6A)**. Intramuscular ECF amplitudes for both control and dehydration animals are normally distributed **(Fig. S6)**. A classifier of measurements performed on animals before (pre) and after (post) dehydration demonstrates strong performance. The AUROC is 0.85 [95% C.I., 0.77 to 0.90]. **(Fig. 6B)**.

The change in the muscle ECF signal from before to after dehydration isolates the effect of fluid depletion while compensating for variability in the initial hydration state of each animal. The change in this signal is significantly greater among dehydration versus control animals ($n = 42$, $p < 0.0011$, statistics by t test). The estimated change in fluid volume attributed to the intramuscular ECF compartment does not show a significant correlation with weight loss in control mice ($n = 9$, $R^2 = 0.035$, $p = 0.632$, statistics by t test) **(Fig. 6C)**. This signal strongly correlates with weight loss in mice that underwent thermal dehydration ($n = 33$, $R^2 = 0.713$, $p < 1\times10^{-9}$, statistics by t test) **(Fig. 6D)**. Residuals of the linear fits do not show any trends with weight loss and are normally distributed **(Fig. S6)**. These results show that the MR signal originating from muscle tissue alone is sufficient to identify and estimate the degree of dehydration. The

change in MR amplitude corresponding to muscle ECF quantifies fluid loss due to dehydration **(Fig. 6D)**. The use of the change in amplitude accounted for the baseline variability observed in the initial hydration state of each animal. Despite this variability, the initial ECF amplitude was moderately correlated with weight loss and the rate of weight loss **(Fig. S7)**. We demonstrate that a multicomponent T2 measurement localized to the muscle tissue is capable of quantifying whole body dehydration.

Portable MR sensor for remote, multicomponent T2 relaxometry

The portable MR sensor reliably demonstrates the linear relationship between transverse relaxation rate and concentration of paramagnetic species ($CuSO_4$) in aqueous solution, a representative synthetic tissue phantom, using a CPMG (Carr-Purcell-Meiboom-Gill) pulse sequence for acquisition ($n = 19$, $R^2 = 0.997$, $p < 1\times10^{-22}$, statistics by t test) **(Fig. 7A)**. There is a linear relationship between sample concentration and estimated relaxation rate across a wide range of concentrations per Bland-Altman analysis ($n = 19$, mean of differences = 0.0008, 95% confidence interval = -0.008 to 0.009, $p = 0.21$, statistics by significance of Spearman rank correlation of means and differences) **(Fig. S8A)**. These results are further confirmed through validation against a gold-standard benchtop NMR spectrometer **(Fig. 7B)**. There is a linear relationship between the estimated relaxation rate from our portable MR sensor and a benchtop NMR spectrometer ($n = 19$, $R^2 = 0.996$, $p = 1\times10^{-12}$, statistics by t test). . There is no bias in estimation of relaxation rates across a wide range of concentrations per Bland-Altman analysis indicating strong agreement ($n = 19$, mean of differences = -0.004, 95% confidence interval = -0.012 to 0.004, $p = 0.70$, statistics by significance of Spearman rank correlation of means and differences) **(Fig. S8B)**.

Relaxation time constants and relative amplitudes of each fluid compartment within the heterogeneous synthetic tissue phantom **(Fig. 8A, inset)** can be accurately and reproducibly extracted from signals acquired by the portable MR sensor via T2 relaxometry **(Fig. 8B-C)**. This exemplifies the ability to accurately quantify fluid distribution across a heterogeneous sample via a single-sided portable MR sensor.

Portable MR measurements of fluid depletion

Our portable MR sensor performs a T2 measurement of the skeletal muscle, similarly to the MRI, which enables isolation and analysis of the signal originating from each tissue fluid compartment. The time-domain relaxometry signal shows a decrease in decay time (pre: 67.1 ms; post: 45.4 ms) after

dehydration, similarly to T2 relaxometry with MRI **(Fig. 9A)**. The ECF component, defined as the amplitude corresponding to the slowest relaxation time in a triexponential fit, was most responsive to fluid depletion **(Fig. 9B)**. The residuals of a triexponential fit are independent and identically distributed with a mean of zero. This suggests that the underlying signal can be completely described by a three-component model. Intramuscular ECF amplitudes for control and dehydration animals are normally distributed **(Fig. S9)**. The muscle ECF compartment amplitude was three times as important as the respective relaxation time in predicting weight loss when assessed via binary decision regression tree analysis **(Fig. S10)**.

The estimated fluid volume attributed to the intramuscular ECF decreases significantly after dehydration ($n = 11$, $p < 0.0104$, statistics by Mann–Whitney U test) while not changing significantly among control animals ($n = 14$, $p < 0.8630$, statistics by t test) **(Fig. 10A)**. A classifier of measurements performed on animals before (pre) and after (post) dehydration demonstrates strong performance. The AUROC is 0.83 [95% C.I., 0.65 to 0.93] **(Fig. 10B)**.

We, once again, analyzed the change in the intramuscular ECF signal from before to after dehydration to isolate the effect of fluid depletion while compensating for variability in the initial hydration state of each animal. The change in this signal is significantly greater among dehydration versus control animals ($n = 25$, $p < 0.0047$, statistics by t test). The estimated change in fluid volume attributed to this compartment does not show a correlation with weight loss in control mice ($n = 14$, $R^2 = 0.044$, $p = 0.471$, statistics by t test) **(Fig. 10C)**. This signal strongly correlates with weight loss ($n = 11$, $R^2 = 0.732$, $p < 0.001$, statistics by t test) in mice that underwent thermal dehydration **(Fig. 10D)**. Residuals of a linear fit do not show any trends with weight loss and are normally distributed **(Fig. S9)**. This shows that a localized measurement within the muscle tissue performed by a single sided portable MR sensor can identify and predict fluid loss induced by thermal dehydration. We experienced limited variability because we perform measurements on a region of the mouse leg which is largely muscle tissue. Repositioning of the mouse leg on top of the sensor was highly controlled. All animals included in the study, additionally, had very similar body mass and composition to reduce anatomical variability.

Discussion

A non-invasive, portable, reliable measurement of fluid volume status would have broad implications for human health (57). Unmanaged disruption of euvolemia is associated with negative health outcomes. The ability to accurately estimate fluid volume status would improve fluid management across diverse patient

populations. These include those experiencing dehydration due to limited fluid intake, environmental exposure, or physical activity; intensive care, emergency department, elderly, and neonatal patients; (1,2,6,8–10,15,58–62). For example, a real-time measure of fluid volume status could inform fluid management in ICU patients. MR-based measurements of local disruptions of tissue fluid distribution have proven clinical utility (41,63,64). Our work extends this to measure systemic fluid depletion via localized measurement of tissue fluid distribution.

We demonstrate the ability to estimate fluid volume depletion through three independent magnetic resonance relaxometry-based measurement techniques: whole animal NMR, MRI, and portable MR. We show that a localized MR measurement performed both via MRI and a portable MR sensor can identify systemic fluid volume status. This suggests the potential for this technology to diagnose dehydration.

Physiology of dehydration

We hypothesized that an MR measurement of intramuscular ECF depletion could identify dehydration. The accepted physiological model of dehydration-induced fluid shifts supports this. Thermal dehydration causes ECF space contraction in humans and rodents (31,65–67). The change in relative volume of extracellular versus total fluid within muscle tissue forms the basis for the MR signal measured with both MRI and the portable MR sensor. The shift in fluids from the extracellular space into the vascular space is driven by osmotic forces and, therefore, the concentration of solutes within the ISF remains approximately unchanged (65,67). We observed a larger change in the MR amplitude of the intramuscular ECF compared to the relaxation rate change. This supports the hypothesis that this measurement is sensitive to relative volume changes of tissue fluid compartments as solute concentration more strongly affects relaxation rate.

The combination of fluid restriction and exposure to a high temperature environment provided rapid fluid loss to directly test our hypothesis while reducing the influence of confounding factors present in other methods of inducing dehydration such as physical activity (68,69). Control animals experienced mean weight loss of 3%, likely due to voiding, variability of food and fluid intake, and changes in metabolism due to diurnal cycle disruption and handling (53–55). No change in MR signal was observed in these euvolemic animals. Experimental animals experienced fluid loss due to thermal exposure in excess of control animals. These animals had weight losses greater than 4% which produces intramuscular ECF compartment contraction. This supports the hypothesis that the intramuscular ECF compartment signal decreases when homeostasis is disturbed and animals must rely upon this fluid compartment to maintain plasma volume.

Dehydration can occur in patients who have lost widely varying amounts of fluid due to body composition variability. A more direct measurement of changes in intramuscular fluid distribution would provide a highly specific measure of dehydration compared to existing clinical diagnostics (blood chemistry, urinalysis, blood pressure, weight). We observed strong correlations between the intramuscular ECF MR signals and weight loss due to highly similar body mass and muscle mass between experimental animals. These findings agree with the physiological model that intramuscular ECF depletes proportionally to fluid loss. A diagnostic of dehydration capable of guiding treatment may only need to identify intramuscular ECF depletion rather than quantify fluid loss.

Our prior study in HD patients showed that excess fluid in hypervolemic patients can be observed by T2 relaxometry localized to skeletal muscle (70). Interestingly, changes in weight and blood chemistry indicated that two healthy control subjects experienced dehydration during this study. MRI of those subjects showed a decrease in the intramuscular ECF signal corresponding to dehydration. The current study was designed to demonstrate the utility of a portable MR sensor via a preclinical model of hyperosmotic dehydration. These results support the proposed explanation from the prior study and suggest that portable MR measurements of intramuscular fluid can identify both dehydration and volume overload in humans.

Advantages of portable MR sensor

The portable MR sensor offers many advantages over traditional MRI. Its miniature size and low power consumption, both realized via permanent magnets, offer a mobile platform capable of performing across a range of environments including hospitals, outpatient facilities, sporting events, and military operations. The device is straightforward to operate as there are no user controlled acquisition parameters. Furthermore, measurement interpretation is fully automated in contrast to traditional MRI. The potential to operate without a trained operator or radiologist for image interpretation may increase accessibility of fluid volume status measurements. Finally, the measurement can be performed in a few minutes suggesting potential for use as a real-time measure of fluid volume status. Portable, single sided MR sensors have recently shown potential across a wide range of biomedical applications (71–75).

Limitations and future work

Several enhancements to the portable MR sensor design and MR pulse sequences would improve measurement accuracy and reduce variability to enhance the potential for clinical translation. The relatively inhomogeneous field and imperfect refocusing flip angle create stimulated echoes and diffusion-weighting biasing T2 estimates (76,77). Pulse sequences that mitigate these effects would allow investigation of relaxation time shifts corresponding to fluid volume status. Changes in diffusivity within the muscle tissue may bias T2-based measurements (78). A sensor capable of performing deeper measurements would be robust to confounding signals from proximal tissue (e.g. subcutaneous). The addition of spatial profiling or diffusion-weighting would isolate the muscle tissue for further analysis. These improvements may allow a future sensor to perform an absolute measure of fluid volume status despite variability in subcutaneous thickness. This would obviate the need for a baseline measurement at euhydration allowing for use as both a monitor of changes in hydration state and an absolute diagnostic of dehydration. A clinical study in a human model of dehydration with an improved sensor could test its clinical utility in a relevant patient population.

Conclusion

We demonstrate a localized measure of tissue fluid distribution using a portable MR device capable of identifying systemic changes in fluid volume status associated with fluid depletion. We validate these findings via whole animal NMR and MRI localized to muscle tissue. Our measurement provides a noninvasive indicator of the fluid volume of distinct fluid compartments and their differential volume contractions during fluid depletion. This method of identifying fluid volume status could serve as a versatile and portable point of care monitoring technique for dehydration.

References

1. Cheuvront SN, Kenefick RW. Dehydration: Physiology, assessment, and performance effects. *Compr Physiol*. 2014;4(1):257-285. doi:10.1002/cphy.c130017
2. Seymour DG, Henschke PJ, Cape RDT, Campbell AJ. Acute confusional states and dementia in the elderly: the role of dehydration/volume depletion, physical illness and age. *Age Ageing*. 1980;9(3):137-146.
3. Chan HYL, Cheng A, Cheung SSS, et al. Association between dehydration on admission and

postoperative complications in older persons undergoing orthopaedic surgery. *J Clin Nurs*. 2018.

4. Lavizzo-Mourey R, Johnson J, Stolley P. Risk factors for dehydration among elderly nursing home residents. *J Am Geriatr Soc*. 1988;36(3):213-218.
5. Thomas DR, Cote TR, Lawhorne L, et al. Understanding clinical dehydration and its treatment. *J Am Med Dir Assoc*. 2008;9(5):292-301. doi:10.1016/j.jamda.2008.03.006
6. Wakefield BJ, Mentes J, Holman JE, Culp K. Risk Factors and Outcomes Associated with Hospital Admission for Dehydration. *Rehabil Nurs*. 2008;33(6):233-241.
7. Creditor MC. Hazards of hospitalization of the elderly. *Ann Intern Med*. 1993;118(3):219-223.
8. Marik PE, Lemson J. Fluid responsiveness: an evolution of our understanding. 2014.
9. Maughan RJ, Shirreffs SM. Development of hydration strategies to optimize performance for athletes in high-intensity sports and in sports with repeated intense efforts. *Scand J Med Sci Sports*. 2010;20:59-69.
10. Lindner G, Funk G-C, Schwarz C, et al. Hypernatremia in the critically ill is an independent risk factor for mortality. *Am J Kidney Dis*. 2007;50(6):952-957.
11. Warren JL, Bacon WE, Harris T, McBean AM, Foley D, Phillips C. The burden and outcomes associated with dehydration among US elderly, 1991. *Am J Public Health*. 1994;84(8):1265-1269.
12. Rolls BJ, Phillips PA. Aging and disturbances of thirst and fluid balance. *Nutr Rev*. 1990;48(3):137-144.
13. FAULL CM, HOLMES C, BAYLIS PH. Water balance in elderly people: is there a deficiency of vasopressin? *Age Ageing*. 1993;22(2):114-120.
14. Phillips PA, Rolls BJ, Ledingham JGG, et al. Reduced thirst after water deprivation in healthy elderly men. *N Engl J Med*. 1984;311(12):753-759.
15. Lindseth PD, Lindseth GN, Petros T V, Jensen WC, Caspers J. Effects of hydration on cognitive function of pilots. *Mil Med*. 2013;178(7):792-798.
16. Hooper L, Abdelhamid A, Attreed NJ, et al. Clinical symptoms, signs and tests for identification of impending and current water-loss dehydration in older people. *Cochrane Database Syst Rev*. 2015;(4).
17. McGee S, Abernethy III WB, Simel DL. Is this patient hypovolemic? *Jama*. 1999;281(11):1022-1029.
18. Gross CR, Lindquist RD, Woolley AC, Granieri R, Allard K, Webster B. Clinical indicators of dehydration severity in elderly patients. *J Emerg Med*. 1992;10(3):267-274. doi:10.1016/0736-4679(92)90331-M
19. Gorelick MH, Shaw KN, Baker MD. Effect of ambient temperature on capillary refill in healthy children. *Pediatrics*. 1993;92(5):699-702.

20. McGarvey J, Thompson J, Hanna C, Noakes TD, Stewart J, Speedy D. Sensitivity and specificity of clinical signs for assessment of dehydration in endurance athletes. *Br J Sports Med*. 2010;44(10):716-719.
21. Gowans EM, Fraser CG. Despite correlation, random spot and 24-h urine specimens are not interchangeable. *Clin Chem*. 1987;33(6):1080-1081.
22. Shephard MD, Penberthy LA, Fraser CG. Short-and long-term biological variation in analytes in urine of apparently healthy individuals. *Clin Chem*. 1981;27(4):569-573.
23. Cheuvront SN, Kenefick RW, Zambraski EJ. Spot urine concentrations should not be used for hydration assessment: A methodology review. *Int J Sport Nutr Exerc Metab*. 2015;25(3):293-297.
24. Harrison MH. Effects on thermal stress and exercise on blood volume in humans. *Physiol Rev*. 1985;65(1):149-209.
25. Cheuvront SN, Kenefick RW, Charkoudian N, Sawka MN. Physiologic basis for understanding quantitative dehydration assessment. *Am J Clin Nutr*. 2013;97(3):455-462. doi:10.3945/ajcn.112.044172
26. Ely BR, Cheuvront SN, Kenefick RW, Sawka MN. *Limitations of Salivary Osmolality as a Marker of Hydration Status*. ARMY RESEARCH INST OF ENVIRONMENTAL MEDICINE NATICK MA THERMAL AND MOUNTAIN MEDICINE DIVISION; 2011.
27. Ellis KJ, Bell SJ, Chertow GM, et al. Bioelectrical impedance methods in clinical research: a follow-up to the NIH Technology Assessment Conference. *Nutrition*. 1999;15(11-12):874-880.
28. Buchholz AC, Bartok C, Schoeller DA. The validity of bioelectrical impedance models in clinical populations. *Nutr Clin Pract*. 2004;19(5):433-446.
29. Kushner RF, Gudivaka R, Schoeller DA. Clinical characteristics influencing bioelectrical impedance analysis measurements. *Am J Clin Nutr*. 1996;64(3):423S-427S.
30. Silverthorn DU, Ober WC, Garrison CW, Silverthorn AC, Johnson BR. *Human Physiology: An Integrated Approach*. Pearson/Benjamin Cummings San Francisco, CA:; 2004.
31. Nose H, Morimoto T, Ogura K. Distribution of water losses among fluid compartments of tissues under thermal dehydration in the rat. *Jpn J Physiol*. 1983;33(6):1019-1029. doi:10.2170/jjphysiol.33.1019
32. Hackney KJ, Cook SB, Fairchild TJ, Ploutz-Snyder LL. Skeletal muscle volume following dehydration induced by exercise in heat. *Extrem Physiol Med*. 2012;1(1):3. doi:10.1186/2046-7648-1-3
33. Costill DL, Fink WJ. Plasma volume changes following exercise and thermal dehydration. *J Appl Physiol*. 1974;37(4):521-525. papers2://publication/uuid/11909E89-3F8F-43B8-97BC-1E7CBB5673F8.

34. Nose H, Mack GW, Shi XR, Nadel ER. Shift in body fluid compartments after dehydration in humans. *J Appl Physiol (Bethesda, Md 1985)*. 1988;65(1):318-324. http://www.ncbi.nlm.nih.gov/pubmed/3403475.
35. Fukushima E, Boden N. *Experimental Pulse NMR: A Nuts and Bolts Approach*. Vol 10. Addison-Wesley; 1982. doi:10.1016/0307-4412(82)90186-8
36. Li M, Vassiliou CC, Colucci LA, Cima MJ. (1)H nuclear magnetic resonance (NMR) as a tool to measure dehydration in mice. *NMR Biomed*. 2015;28(8):1031-1039. doi:10.1002/nbm.3334
37. Saab G, Thompson RT, Marsh GD. Multicomponent T 2 Relaxation of In Vivo Skeletal Muscle. *Magn Reson Med*. 1999;157(1999):150-157. doi:10.1002/(SICI)1522-2594(199907)42:1<150::AID-MRM20>3.0.CO;2-5
38. Harrison R, Bronskill MJ, Mark Henkelman R. Magnetization transfer and T2 relaxation components in tissue. *Magn Reson Med*. 1995;33(4):490-496.
39. English AE, Joy MLG, Henkelman RM. Pulsed NMR relaxometry of striated muscle fibers. *Magn Reson Med*. 1991;21(2):264-281.
40. Cole WC, LeBlanc AD, Jhingran SG. The origin of biexponential T2 relaxation in muscle water. *Magn Reson Med*. 1993;29(1):19-24. doi:10.1002/mrm.1910290106
41. Ababneh Z, Beloeil H, Berde CB, Gambarota G, Maier SE, Mulkern R V. Biexponential parameterization of diffusion and T2 relaxation decay curves in a rat muscle edema model: decay curve components and water compartments. *Magn Reson Med An Off J Int Soc Magn Reson Med*. 2005;54(3):524-531. doi:10.1002/mrm.20610
42. Gambarota G, Cairns BE, Berde CB, Mulkern R V. Osmotic effects on the T2 relaxation decay of in vivo muscle. *Magn Reson Med An Off J Int Soc Magn Reson Med*. 2001;46(3):592-599.
43. Araujo ECA, Fromes Y, Carlier PG. New insights on human skeletal muscle tissue compartments revealed by in vivo T2 NMR relaxometry. *Biophys J*. 2014;106(10):2267-2274.
44. Colucci LA, Corapi KM, Li M, et al. Fluid assessment in dialysis patients by point-of-care magnetic relaxometry. *Sci Transl Med*. 2019;11(502):eaau1749.
45. Bashyam A, Frangieh CJ, Cima MJ. Portable, single-sided magnetic resonance sensor for hydration status assessment via multicomponent T2 relaxometry. In: *Proc. the International Society of Magnetic Resonance in Medicine (ISMRM)*. Montreal, Canada; 2019.
46. Bashyam A, Li M, Cima MJ. Design and experimental validation of Unilateral Linear Halbach magnet arrays for single-sided magnetic resonance. *J Magn Reson*. 2018;292:36-43. doi:10.1016/j.jmr.2018.05.004
47. Eidmann G, Savelsberg R, Blümler P, Blümich B. The NMR MOUSE, a mobile universal surface explorer. *J Magn Reson Ser A*. 1996;122(1):104-109.

48. Casanova F, Perlo J, Blümich B. *Single-Sided NMR*. (Casanova F, Perlo J, Blümich B, eds.). Berlin, Heidelberg: Springer Berlin Heidelberg; 2011. doi:10.1007/978-3-642-16307-4
49. Prado PJ, Blümich B, Schmitz U. One-Dimensional Imaging with a Palm-Size Probe. *J Magn Reson*. 2000;144(2):200-206. doi:10.1006/jmre.2000.2038
50. Blümich B, Anferov V, Anferova S, et al. Simple NMR-MOUSE with a bar magnet. *Concepts Magn Reson Part B Magn Reson Eng*. 2002;15(4):255-261. doi:10.1002/cmr.10046
51. Blümich B, Casanova F, Perlo J, et al. Advances of unilateral mobile NMR in nondestructive materials testing. *Magn Reson Imaging*. 2005;23(2):197-201.
52. Möller R, Tafeit E, Pieber TR, Sudi K, Reibnegger G. Measurement of subcutaneous adipose tissue topography (SAT-Top) by means of a new optical device, LIPOMETER, and the evaluation of standard factor coefficients in healthy subjects. *Am J Hum Biol Off J Hum Biol Assoc*. 2000;12(2):231-239.
53. Deacon RMJ. Housing, husbandry and handling of rodents for behavioral experiments. *Nat Protoc*. 2006;1(2):936.
54. Ellacott KLJ, Morton GJ, Woods SC, Tso P, Schwartz MW. Assessment of feeding behavior in laboratory mice. *Cell Metab*. 2010;12(1):10-17.
55. NAKAMURA Y, SUZUKI K. Tunnel use facilitates handling of ICR mice and decreases experimental variation. *J Vet Med Sci*. 2018;80(6):886-892.
56. Bai R, Koay CG, Hutchinson E, Basser PJ. A framework for accurate determination of the T2 distribution from multiple echo magnitude MRI images. *J Magn Reson*. 2014;244:53-63. doi:10.1016/j.jmr.2014.04.016
57. Armstrong LE, Amstrong L. Assesing Hydration Status : The Elusive Gold Standard. *J Am Coll Nutr*. 2007;26(5):26 (14): 575-84.
58. Xiao H, Barber J, Campbell ES. Economic burden of dehydration among hospitalized elderly patients. *Am J Heal Pharm*. 2004;61(23):2534-2540.
59. Bolat F, Oflaz MB, Güven AS, et al. What Is the Safe Approach for Neonatal Hypernatremic Dehydration?: A Retrospective Study From a Neonatal Intensive Care Unit. *Pediatr Emerg Care*. 2013;29(7):808-813.
60. Luippold AJ, Charkoudian N, Kenefick RW, et al. Update: Efficacy of Military Fluid Intake Guidance. *Mil Med*. 2018.
61. Messaris E, Sehgal R, Deiling S, et al. Dehydration is the most common indication for readmission after diverting ileostomy creation. *Dis Colon Rectum*. 2012;55(2):175-180.
62. Sands JJ, Usvyat LA, Sullivan T, et al. Intradialytic hypotension: frequency, sources of variation and correlation with clinical outcome. *Hemodial Int*. 2014;18(2):415-422.

63. Garcia J. MRI in inflammatory myopathies. *Skeletal Radiol*. 2000;29(8):425-438.
64. Meler JD, Solomon M a, Steele JR, Yancy CW, Parkey RW, Fleckenstein JL. The MR appearance of volume overload in the lower extremities. *J Comput Assist Tomogr*. 1997;21(6):969-973. doi:10.1097/00004728-199711000-00022
65. Darrow DC, Yannet H. The changes in the distribution of body water accompanying increase and decrease in extracellular electrolyte. *J Clin Invest*. 1935;14(2):266-275.
66. Mange K, Matsuura D, Cizman B, et al. Language guiding therapy: the case of dehydration versus volume depletion. *Ann Intern Med*. 1997;127(9):848-853.
67. Nadal JW, Pedersen S, Maddock WG. A comparison between dehydration from salt loss and from water deprivation. *J Clin Invest*. 1941;20(6):691-703.
68. Fleckenstein JL, Canby RC, Parkey RW, Peshock RM. Acute effects of exercise on MR imaging of skeletal muscle in normal volunteers. *Am J Roentgenol*. 1988;151(2):231-237.
69. Ploutz-Snyder LL, Convertino VA, Dudley GA. Resistance exercise-induced fluid shifts: change in active muscle size and plasma volume. *Am J Physiol Integr Comp Physiol*. 1995;269(3):R536-R543.
70. Colucci LA, Corapi KM, Li M, et al. Bedside magnetic relaxometry for fluid assessment in end-stage renal disease. *under Rev*. 2019.
71. Ali TS, Tourell MC, Hugo HJ, et al. Transverse relaxation-based assessment of mammographic density and breast tissue composition by single-sided portable NMR. *Magn Reson Med*. 2019.
72. He Z, He W, Wu J, Xu Z. The novel design of a single-sided MRI probe for assessing burn depth. *Sensors*. 2017;17(3):526.
73. Tourell MC, Ali TS, Hugo HJ, et al. T1-based sensing of mammographic density using single-sided portable NMR. *Magn Reson Med*. 2018;80(3):1243-1251.
74. Petrov O V, Stapf S. Multicomponent analysis of T1 relaxation in bovine articular cartilage at low magnetic fields. *Magn Reson Med*. 2019;81(5):2858-2868.
75. Brizi L, Barbieri M, Baruffaldi F, et al. Bone volume–to–total volume ratio measured in trabecular bone by single-sided NMR devices. *Magn Reson Med*. 2018;79(1):501-510.
76. Burstein D. Stimulated echoes: Description, applications, practical hints. *Concepts Magn Reson*. 1996;8(4):269-278.
77. Pell GS, Briellmann RS, Waites AB, Abbott DF, Lewis DP, Jackson GD. Optimized clinical T2 relaxometry with a standard CPMG sequence. *J Magn Reson Imaging*. 2006;23(2):248-252.
78. Radunsky D, Blumenfeld-Katzir T, Volovyk O, et al. Analysis of magnetization transfer (MT) influence on quantitative mapping of T2 relaxation time. *Magn Reson Med*. 2019.

Acknowledgements

We thank the Koch Institute Swanson Biotechnology Center for technical support, specifically Wei Huang and Virginia Spanoudaki at Animal Imaging and Preclinical Testing. We thank Gregory Ekchian, Richard Joshua Murdock, Max Cotler, Aaron Baggish, Dennis Ausiello, Matthew Rosen, and Elfar Adalsteinsson for helpful discussions; Elizabeth Zhang, Connor Stashko, Alex Lim, and Brooke McGoldrick for assistance with instrumentation and experimental support. **Funding:** This work was supported in part by MIT Institute for Soldier Nanotechnologies (United States Army Research Office Grant W911NF-13D-0001); National Institutes of Health – National Cancer Institute Centers of Cancer Nanotechnology Excellence Grant U54 CA151884-02, and the Koch Institute Support (core) grant P30-CA14051 from the National Cancer Institute. AB was supported by a Fannie & John Hertz Foundation Graduate Fellowship and a National Science Foundation Graduate Fellowship. **Author contributions:** A.B. and M.L. designed and constructed the portable MR sensor. A.B. and C.J.F. characterized the portable MR sensor and conducted all animal experiments. A.B. analyzed the data, prepared figures, and wrote the manuscript. A.B., C.J.F., and M.J.C. designed the experiments, and interpreted results. A.B., C.J.F., M.L., and M.J.C. edited the manuscript. M.J.C. supervised the research. **Competing interests:** A.B., M.L., and M.J.C. are inventors on a patent application (US20180306879) submitted by MIT that describes the design of the permanent magnet array within the portable MR sensor. M.L. and M.J.C. are inventors on a patent application (US20160120438) submitted by MIT that describes the methods to determine hydration state utilized herein. **Data and materials availability:** The data sets, materials, and analysis generated during the current study are available from the corresponding author on reasonable request.

Figure Captions

Fig. 1. Schematic illustration of mouse thermal dehydration model. A-B) Experimental mice were exposed to a 37 C, 15-20% relative humidity, and high airflow environment. Urine and feces were collected in a 96-well plate. MR measurements were performed before and after dehydration.

Fig. 2. Portable MR sensor design and field characterization. A) Fully assembled sensor with RF matching circuit and solenoidal transceiver coil. **B)** Illustration of Unilateral Linear Halbach permanent

magnet array design for sensor. Red and grey shading indicates positive and negative poles, respectively, of each magnet. **C)** Measured static magnetic field profile directly above center of magnet. Shaded region indicates predicted sensitive region.

Fig. 3. Portable MR sensitivity profile characterization. A-B) Illustration of sensitivity profile characterization of portable MR sensor. Experimental schematic for MR sensor sensitivity profiles along **A)** xz-plane and **B)** yz-plane. **C-D)** Relative sensitivity of sensor across the **C)** xz-plane and the **D)** yz-plane indicates a 12 × 5 × 2 mm sensitive region. Shaded green and blue planes in **(Figure 2B)** indicate relative orientation of measurement planes. Dashed lines indicate 50% relative sensitivity from the peak of the measurement region.

Fig. 4 Skeletal muscle localization via portable MR sensor. A) Illustration of portable MR sensor with upper leg of mouse positioned over sensitive region. Blue plane indicates approximate orientation of MR image shown in (b). **B)** T2-weighted axial MRI of a mouse leg with overlaid sensitivity profile from portable MR sensor. Yellow, orange, and red contours indicate 25%, 50%, and 75% of max sensitivity, respectively.

Fig. 5. T2 relaxometry with MRI localized to the muscle identifies fluid depletion due to thermal dehydration. A) T2-weighted MRI of the upper leg muscle in a mouse oriented along the coronal plane with overlaid region of interest of muscle tissue. **B)** Decay curves from T2 relaxometry acquired via MRI before and after dehydration show a difference in decay rate. Inset highlights this difference as greatest between 80 and 300 ms.

Fig. 6. T2 relaxometry with MRI localized to the muscle quantifies fluid depletion due to thermal dehydration. A) The amplitude of the second peak in a biexponential fit with fixed time constants, corresponding to the intramuscular ECF signal, significantly decreases after dehydration ($n = 33$, $p < 1\times10^{-6}$, statistics by t test). Control animals did not exhibit a significant change ($n = 9$, $p < 0.5820$, statistics by t test). **B)** A ROC curve of a classifier of pre versus post measurements among dehydrated animals via logistic regression demonstrates an AUROC of 0.85 [95% C.I., 0.77 to 0.90]. Shaded region indicates 95% confidence intervals. **C)** There is no significant correlation between the change in the intramuscular ECF signal amplitude and weight loss in control animals ($n = 9$, $R^2 = 0.035$, $p = 0.632$, statistics by t test). **D)** The change in this signal significantly correlates with weight loss induced by

dehydration (n = 33, $R^2 = 0.713$, $p < 1\times10^{-9}$, statistics by t test). Shaded regions indicate 95% confidence intervals for linear fit (y-intercept 8.8 ± 3.8%, slope -2.5 ± 0.6 %/%).

Fig. 7. Validation of T2 relaxometry via portable MR sensor. A) Linearity of R2 relaxometry measurements with portable MR sensor versus paramagnetic species concentration. Shaded region indicates the standard deviation of the error of the linear fit (n = 19, $R^2 = 0.997$, $p < 1\times10^{-22}$, statistics by t test). **B)** The estimated relaxation rates for portable MR sensor versus benchtop NMR spectrometer are linearly related (n = 19, $R^2 = 0.996$, $p = 1\times10^{-12}$, statistics by t test). Shaded region indicates the standard deviation of the error of the linear fit. Residuals of a linear fit between the relaxation rate estimates between the two MR systems are approximately normally distributed (n = 19, p = 0.768, Lilliefors test for normality).

Fig. 8. Portable MR sensor identifies and quantifies fluid compartments via multicomponent T2 relaxometry. A) MR signal acquired with CPMG acquisition from a synthetic tissue phantom comprising equal parts fast (24 ms, dark blue) and slow (84 ms, light blue) fluid compartments. Inset illustrates cross section of phantom. **B-C)** Analysis of each component with a biexponential model demonstrates accurate identification and quantification of the decay rate (τ_A, τ_B) and relative amplitude (A_A, A_B) of each component. Repeated trials yield histograms of estimation error.

Fig. 9. T2 relaxometry with portable MR sensor identifies fluid depletion due to thermal dehydration. A) T2 relaxometry decay curves localized towards muscle with portable MR sensor before and after dehydration show a difference in decay rate. Inset highlights greatest difference between 40 and 200 ms. **B)** Dehydration induces a shift in the amplitude of the third peak in a triexponential fit **(Eq. (2))**. Colors indicate weight loss induced by dehydration.

Fig. 10. T2 relaxometry with portable MR sensor quantifies fluid depletion due to thermal dehydration. A) The amplitude of the second peak, corresponding to the intramuscular ECF signal, significantly decreases after dehydration (n = 11, $p < 0.0104$, statistics by Mann–Whitney U test). Control animals did not exhibit a significant change (n = 14, $p < 0.8630$, statistics by t test). **B)** A ROC curve of a classifier of pre versus post measurements among dehydrated animals via logistic regression demonstrates an AUROC of 0.83 [95% C.I., 0.65 to 0.93]. Shaded region indicates 95% confidence intervals. **C)** There is no significant correlation between the change in the intramuscular ECF signal amplitude and weight

loss in control animals (n = 14, $R^2 = 0.044$, p = 0.471, statistics by t test). **D)** The change in this signal significantly correlates with weight loss induced by dehydration (n = 11, $R^2 = 0.732$, $p < 0.001$, statistics by t test). Shaded regions indicate 95% confidence intervals for linear fit (y-intercept 38.0 ± 9.4%, slope -5 ± 2.3 %/%).

Supporting Information Captions

Fig. S1. Static magnetic field profile characterization of portable MR sensor. A) Simulated field profile directly above the center of the magnet, indicated by blue plane in **(Fig. 2B)**. Shaded region indicates predicted sensitive region assuming a transceiver coil sensitive to a region approximately 10mm wide with a bandwidth of ±1%. **B-C)** magnetic field strength deviation from B0 along y-axis and z-axis, respectively, through the center of uniform region. Shaded regions correspond to ±1% deviation from B0.

Fig. S2. Whole animal NMR T2 relaxometry quantifies fluid loss in a mouse model of thermal dehydration. A) T2 decay curves from whole animal NMR before and after dehydration show a difference in decay time (pre: 96.7 ms; post: 88.0 ms). Inset highlights this difference as greatest between 50 and 250 ms. **B)** Dehydration induces a shift in the relaxation time and amplitude corresponding to the second peak in a three component exponential fit corresponding to lean muscle tissue. **C)** Amplitude of second component, corresponding to lean muscle tissue, is an approximately 2.8 times more important predictor of weight loss than the respective relaxation time. **D)** The amplitude of the second peak in a triexponential fit with fixed time constants, corresponding to the muscle signal, significantly decreases after dehydration (n = 47, $p < 1\times10^{-15}$, statistics by t test). Control animals did not exhibit a significant change (n = 11, $p < 0.1241$, statistics by t test). Lean muscle tissue amplitudes for control and dehydration animals are normally distributed **(Fig. S3)**. **E)** A receiver operator characteristic (ROC) curve of a binary classifier of pre versus post measurements among dehydrated animals via logistic regression demonstrates an AUROC of 0.93 [95% C.I., 0.88 to 0.96]. Shaded region indicates 95% confidence intervals. **F)** The change in MR amplitude corresponding to the muscle signal is significantly greater among dehydration versus control animals. (n = 58, $p < 1\times10^{-8}$, statistics by t test). **G)** There is no significant correlation between the change in muscle signal amplitude and weight loss in control animals (n = 11, $R^2 = 0.000$, p = 0.996, statistics by t test). **H)** The change in muscle signal amplitude demonstrates sensitivity towards weight loss induced by dehydration (n = 47, $R^2 = 0.616$, $p < 1\times10^{-10}$, statistics by t test). Residuals of the linear fits do not show any trends with weight loss and are normally distributed **(Fig. S3)**. Shaded regions

indicate 95% confidence intervals for linear fit. These results show that the MR signal originating from the lean muscle tissue alone is sufficient to identify and estimate the degree of dehydration.

Fig. S3. Statistics for amplitude of second component from whole animal NMR and linear fits. The amplitude of the second component is approximately normally distributed for **A)** before dehydration (pre) (DHY: n = 47, p = 0.5512; CTL: n = 11, p = 0.4423) and **B)** after dehydration (post) (DHY: n = 47, p = 0.3528; CTL: n = 11, p = 0.7466) measurements. **C)** The change in this amplitude from before to after dehydration is also approximately normally distributed (DHY: n = 47, p = 0.6320; CTL: n = 11, p = 0.7042). All statistics are by Lilliefors test for normality. Residuals for linear fits for control (CTL) and dehydration (DHY) whole animal NMR scans **D-E)** do not show any trends dependent on weight loss and **F)** are approximately normally distributed (CTL: n = 11, p = 0.6742; DHY: n = 47, p = 0.3625, Lilliefors test for normality).

Fig. S4. Illustration of T2 relaxometry via a series of spin echo MR images. A-F) Spin echo images acquired at increasing echo times (TE) show increased signal attenuation due to T2 relaxation. Voxels corresponding to tissues with a longer T2 (e.g. fat) lose brightness at a slower rate than those corresponding to a shorter TE (e.g. muscle). **G-H)** Acquiring images at many TEs provides a sufficient number of echoes to visualize distinct decay curves and extract relaxation parameters for each tissue. Decay curves corresponding to the sum of all echoes within each ROI across all TEs are shown on g) linear and h) log plots. Dashed lines indicate the TEs to which the images **(A-F)** correspond.

Fig. S5. Correction of Rician noise from MRI echoes improves accuracy of parameter estimates from exponential fits. A) Representative uncorrected and corrected T2 decays from a series of spin echo images with an MRI. **B)** Histograms of the noise amplitude in uncorrected and corrected decays shows a positive bias before correction. **C)** A monoexponential fit performed on uncorrected and corrected synthetic decay curves shows a significant improvement in relaxation time estimation accuracy for corrected data. The shaded regions correspond to 95% confidence intervals upon repeated trials (n = 100 trials per SNR level).

Fig. S6. Statistics for amplitude of second component from MRI and linear fits. The amplitude of the second component is approximately normally distributed for **A)** before dehydration (pre) (DHY: n = 33, p = 0.4598; CTL: n = 9, p = 0.9344) and **B)** after dehydration (post) (DHY: n = 33, p = 0.5782; CTL: n = 9, p = 0.6636) measurements. **C)** The change in this amplitude from before to after dehydration is also

approximately normally distributed (DHY: n = 33, p = 0.6062; CTL: n = 9, p = 0.4246). All statistics are by Lilliefors test for normality. Residuals for linear fits for control (CTL) and dehydration (DHY) T2 relaxometry scans with MRI on muscle **D-E)** do not show any trends dependent on weight loss and **F)** are approximately normally distributed (CTL: n = 9, p = 0.5190; DHY: n = 33, p = 0.4031, Lilliefors test for normality).

Fig. S7. Predicting weight loss with initial MRI muscle ECF amplitude. A-D) The correlation between the muscle ECF amplitude from MRI before dehydration and each weight loss feature. The initial muscle ECF amplitude is correlated with each of the respective features derived from the weight loss time series data. The positive correlations with weight loss **(A, C, D)** indicate an increased capacity for fluid loss in animals exhibiting large values for initial muscle ECF amplitude. The negative correlation with time **(B)** indicates an increased weight loss rate in animals exhibiting large values for initial muscle ECF amplitude.

Fig. S8. Validation of T2 relaxometry measurements from portable MR sensors. A) Bland-Altman analysis for linear fit of paramagnetic species concentration versus relaxation rate from portable MR sensor. Residuals of linear fit for estimated relaxation rate do not show any trends dependent on paramagnetic species concentration. Residuals of a linear fit are approximately normally distributed (n = 19, p = 0.768, Lilliefors test for normality). Bland-Altman analysis indicates a linear relationship between sample concentration and estimated relaxation rate across a wide range of concentrations (n = 19, mean of differences = 0.0008, 95% confidence interval = -0.008 to 0.009, p = 0.21, statistics by significance of Spearman rank correlation of means and differences). **Validation of T2 relaxometry measurements from portable MR sensor with benchtop NMR spectrometer. B)** There is no bias in estimation of relaxation rates across a wide range of concentrations per Bland-Altman analysis indicating strong agreement between the two measurements (n = 19, mean of differences = -0.004, 95% confidence interval = -0.012 to 0.004, p = 0.70, statistics by significance of Spearman rank correlation of means and differences).

Fig. S9. Statistics for amplitude of second component from portable MR sensor and linear fits. The amplitude of the second component is approximately normally distributed for **A)** before dehydration (pre) (DHY: n = 11, p = 0.4558; CTL: n = 14, p = 0.8013) and **B)** after dehydration (post) for only control measurements (DHY: n = 11, p = 0.0308; CTL: n = 14, p = 0.7398) measurements. **C)** The change in this amplitude from before to after dehydration is also approximately normally distributed (DHY: n = 11, p =

0.5397; CTL: n = 14, p = 0.8306). All statistics are by Lilliefors test for normality. Residuals for linear fits for control (CTL) and dehydration (DHY) portable MR scans **D-E)** do not show any trends dependent on weight loss and **F)** are approximately normally distributed (CTL: n = 14, p = 0.7755; DHY: n = 11, p = 0.3801, Lilliefors test for normality).

Fig. S10. Identification of strongest predictor of weight loss from portable MR measurements. The amplitude of the second component of portable MR sensor measurements, corresponding to ECF, was an approximately 3.2 times more important predictor of weight loss than the respective relaxation time. Predictor importance was calculated by estimating the change in mean squared error attributed to the inclusion of each predictor in a binary regression decision tree. Error bars indicate standard error of the mean across all models generated via 10-fold cross validation.

Fig. S11. Impedance matching circuit design and performance characterization. A) RF impedance matching circuit schematic using an "L" topology. **B)** Reflected signal versus frequency when tuned to a single operating frequency. Inset highlights the ability to reach a very low reflection coefficient at a desired frequency.

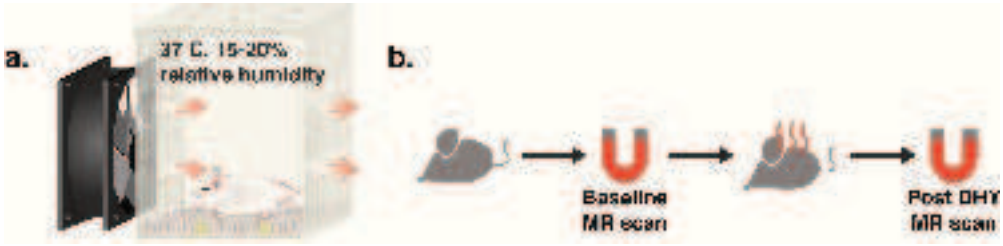

mrm_28004_f1.tif

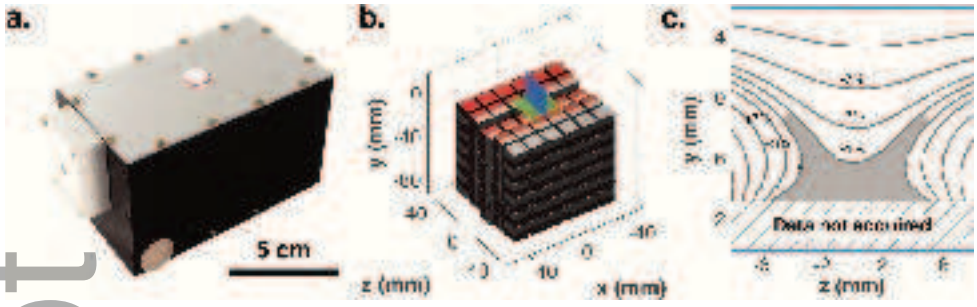

mrm_28004_f2.tif

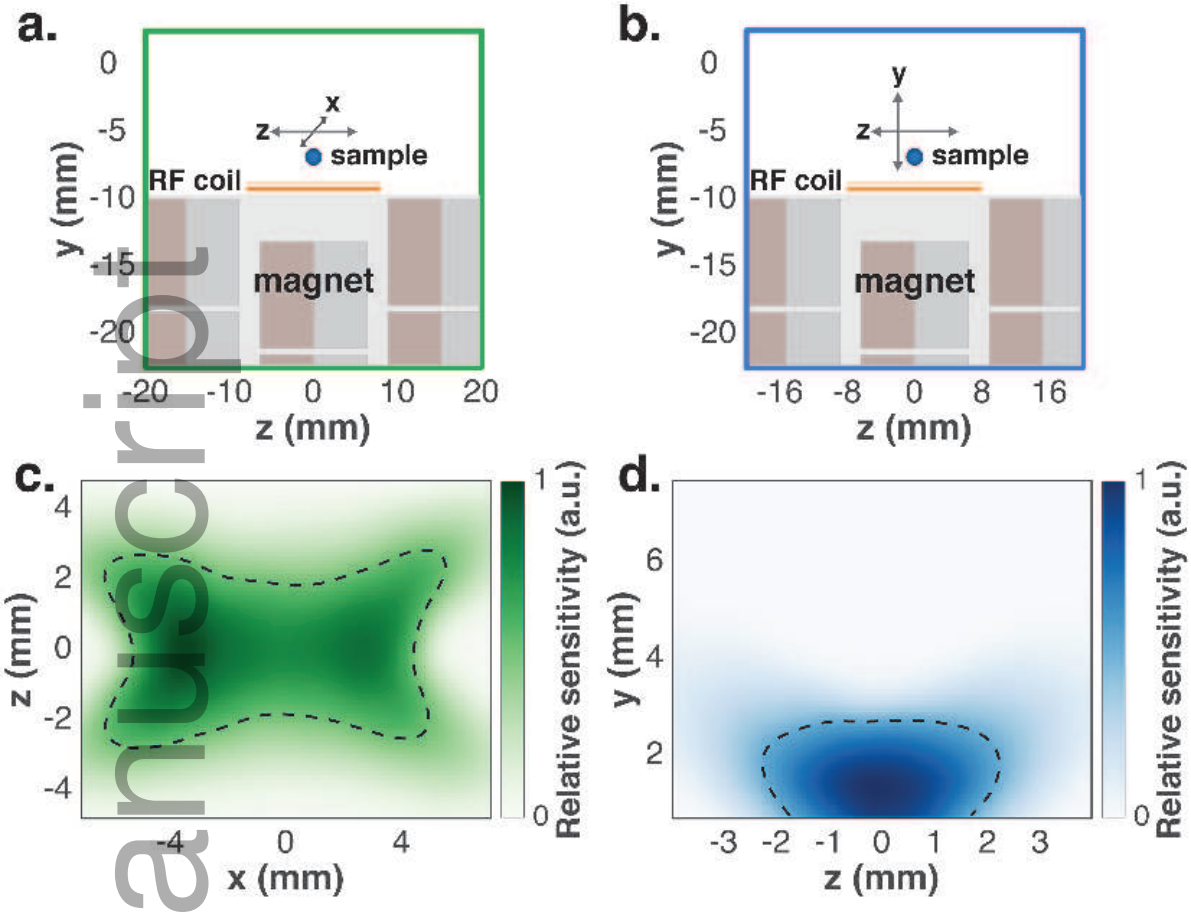

mrm_28004_f3.tif

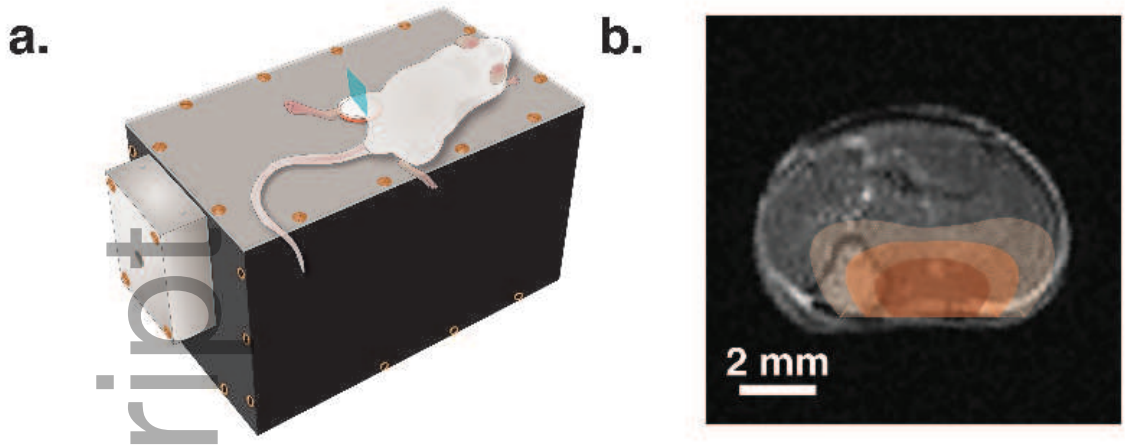

mrm_28004_f4.tif

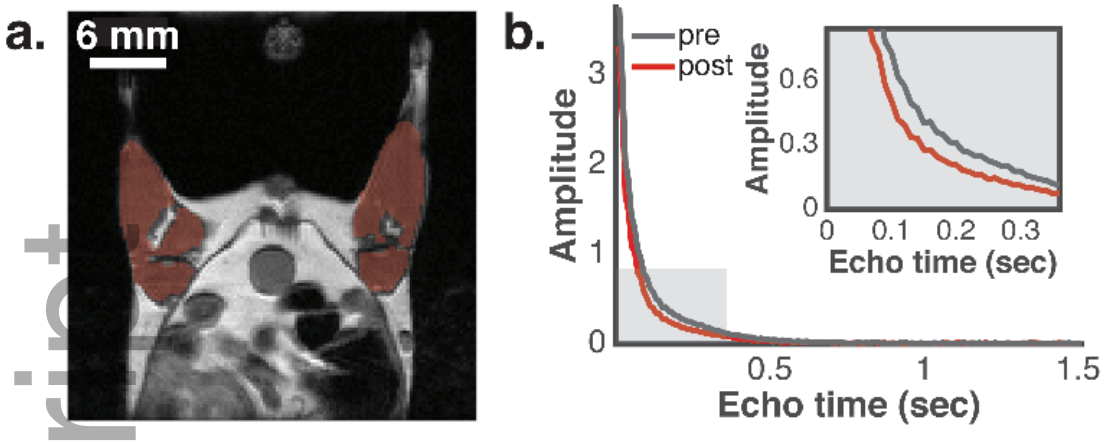

mrm_28004_f5.tif

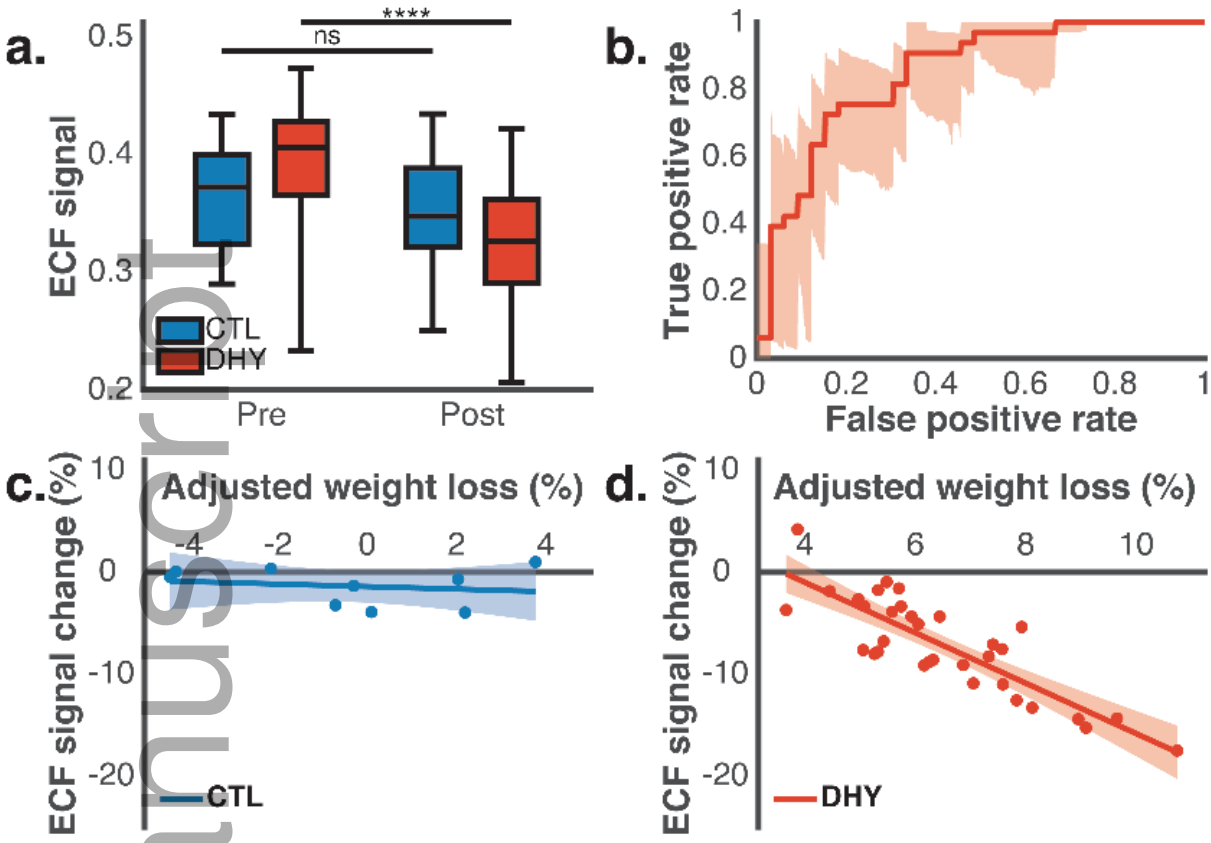

mrm_28004_f6.tif

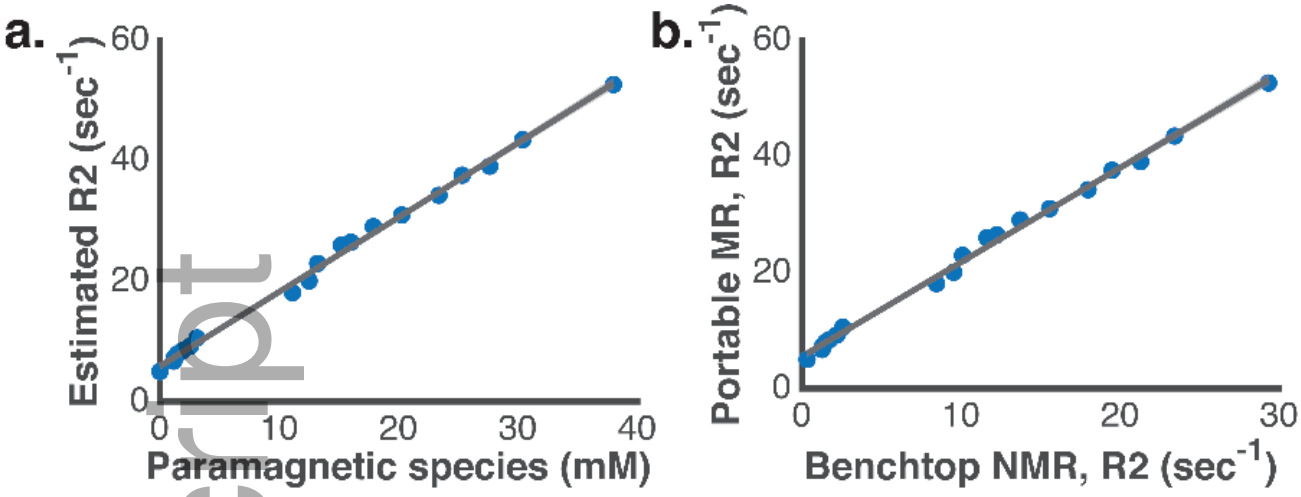

mrm_28004_f7.tif

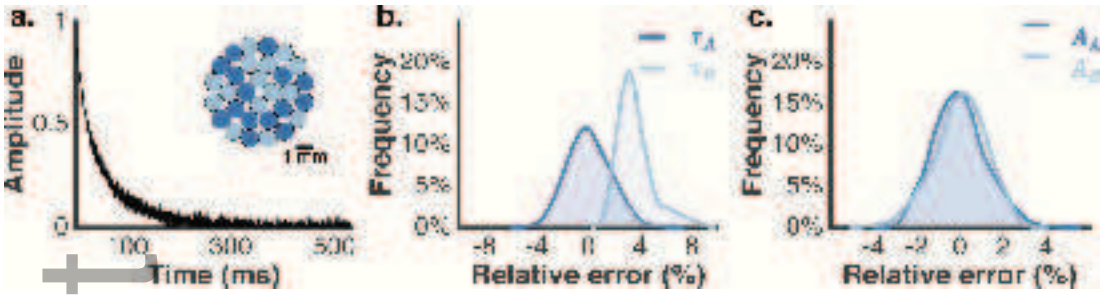

mrm_28004_f8.tif

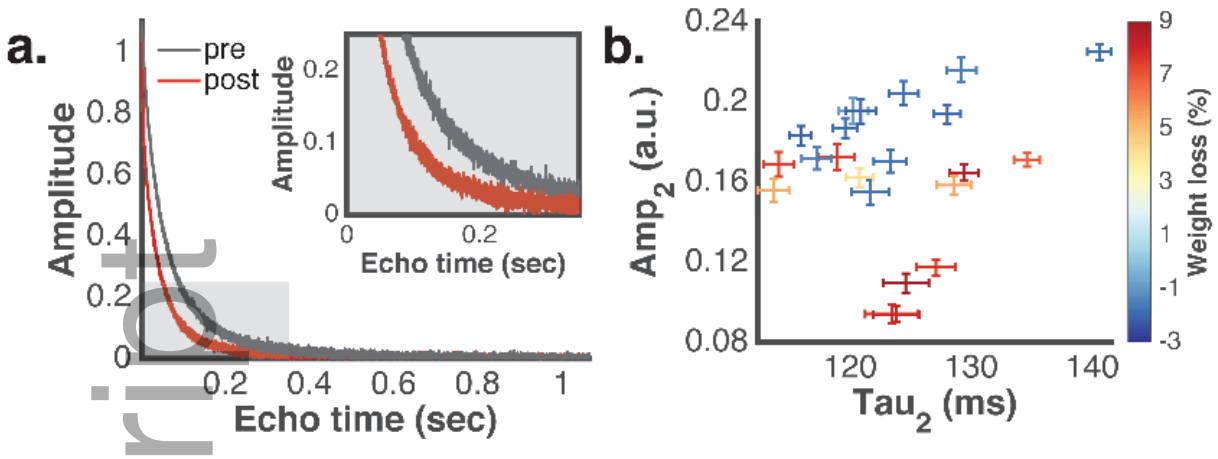

mrm_28004_f9.tif

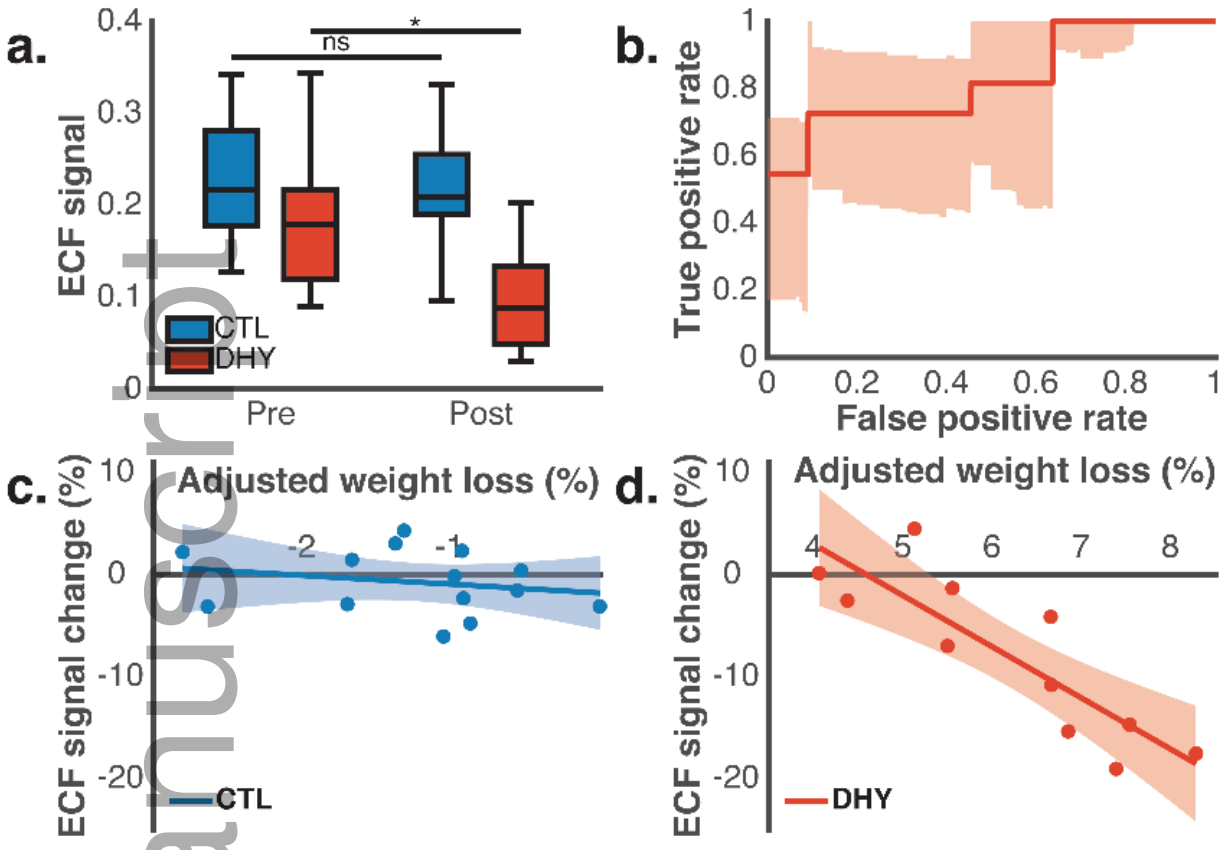

mrm_28004_f10.tif